Electronic Supplementary Material (ESI) for Journal of Materials Chemistry A.

This journal is © The Royal Society of Chemistry 2022

Ir/Ni-NiO/CNT Composites as Effective Electrocatalysts for Hydrogen Oxidation

Xiafang Ji,[a] Peng Chen,[a] Yuanjun Liu,[b] Zhenyuan Ji,[a] Hongbo Zhou,[a,*] Cairao Chen,[a] Xiaoping Shen,[a] Xiaoqi Fu,[a] and Guoxing Zhu[a,*]

[a]School of Chemistry and Chemical Engineering, Jiangsu University, Zhenjiang 212013, China.

[b]School of Environmental and Chemical Engineering, Jiangsu University of Science and Technology, Zhenjiang 202018, China

Corresponding authors:

Email: zhouhb@ujs.edu.cn; zhuguoxing@ujs.edu.cn

Supplementary methods

HOR polarization curves at different rotating rates (2500, 1600, 900, and 400 rpm) were conducted to extract the kinetic current density (j^k) of each catalyst from the Koutecky-Levich equation (Eq. 1),[s1-s3]

$$\frac{1}{j}=\frac{1}{j^k}+\frac{1}{j^d}=\frac{1}{j^k}+\frac{1}{Bc_0\omega^{1/2}} \qquad \text{Eq. 1}$$

where j is the measured current density, j^d is the diffusion limited current density, B is the Levich constant, c_0 is the solubility of H_2 (7.33×10^{-4} mol L^{-1}), ω is the rotating speed, respectively. Among them, B could be calculated from Eq. 2,

$$B = 0.62nFD^{2/3}v^{-1/6} \qquad \text{Eq. 2}$$

where n is the electron transfer number, F is the Faraday constant (96485 C mol^{-1}), D is the diffusivity of H_2 (3.7×10^{-5} cm^2 s^{-1}), and v is the kinematic viscosity (1.01×10^{-2} cm^2 s^{-1}).

Exchange current density (j^0) was deduced from the Butler-Volmer equation (Eq. 3),

$$j^0 = \frac{RTj}{F\eta} \quad \text{Eq. 3}$$

j^0 can be obtained by fitting the kinetic current into the linearized Butler-Volmer equation (Eq. 3), where R is the universal gas constant (8.314 J mol^{-1} K^{-1}), T is the operating temperature (298.15 K), F is the Faraday constant (96485 C mol^{-1}).

Electrochemical active surface areas (ECSAs) were estimated via Cu underpotential deposition (UPD) stripping for all samples after HOR tests.[s4] The catalysts were firstly cycled in Ar-saturated 0.1 M H_2SO_4 solution to guarantee a repeatable voltammogram curve as the background, and then were kept at 0.30 V (vs RHE) for 100 s in an Ar-saturated 0.1 M H_2SO_4 solution containing 2 mM $CuSO_4$. UPD Cu oxidation polarization curve was performed from 0.30 to 1.10 V with a scan rate of 10 mV s^{-1}. The ECSAs were calculated via Eq. 4,

$$ECSA = \frac{Q_{Cu}}{Q_s m_{metal}} \quad \text{Eq. 4}$$

where Q_{Cu} stands the measured integral charge, Q_s represents the surface charge density of 420 μC cm_{metal}^{-2} for monolayer adsorption of Cu-UPD stripping, m_{metal} is the mass of the metal on GC.

Supplementary figures

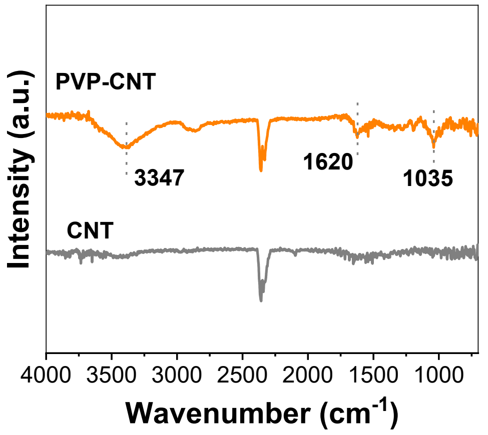

Fig. S1. FT-IR spectra of PVP-CNT and pristine CNT.

The PVP-functionalized CNTs were examined by FT-IR spectrum, which presents three main absorption peaks. The peak at 3347 cm^{-1} is related to the O-H stretching vibrations of hydroxyl groups. The peaks at 1620 and 1035 cm^{-1} are relevant to the C=O and C-N stretching vibrations of the carboxyl moieties. The existence of polar functional groups indicates the improvement of hydrophilicity and the successful functionalization of CNTs.

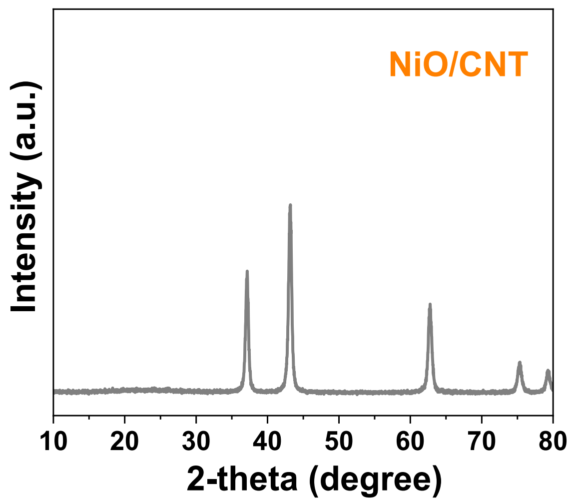

Fig. S2. XRD pattern of NiO/CNT product.

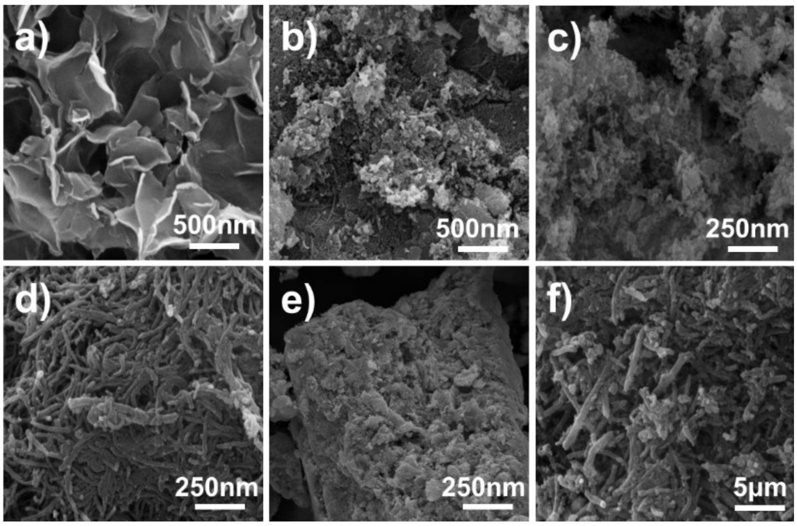

Fig. S3. SEM images for a) $Ni(OH)_2$/CNT, b) NiO/CNT, c) *tre*-NiO/CNT, d) Ir/CNT and e-f) Ir/Ni-NiO/CNT.

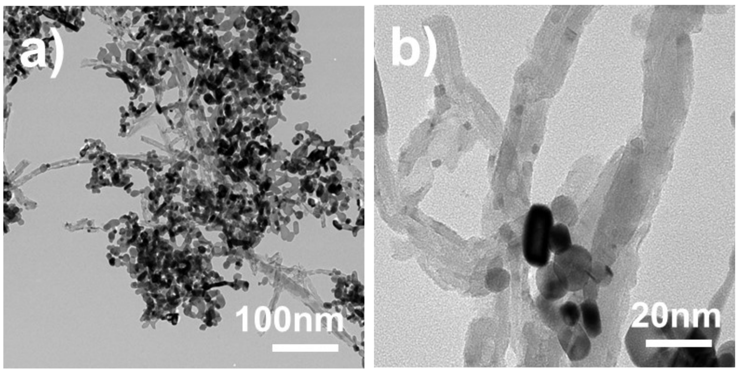

Fig. S4. TEM images of *tre*-NiO/CNT.

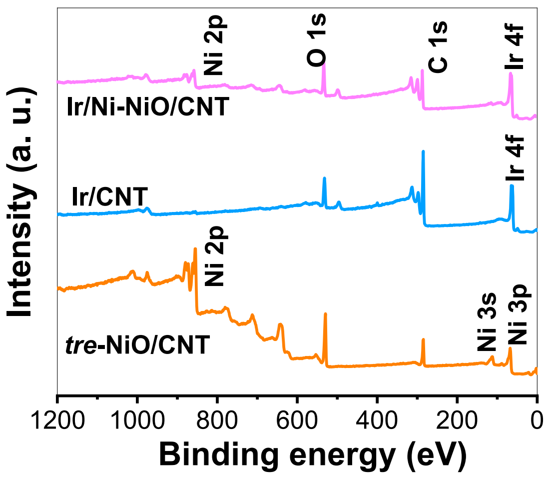

Fig. S5. The survey scan XPS spectra of *tre*-NiO/CNT, Ir/CNT, and Ir/Ni-NiO/CNT.

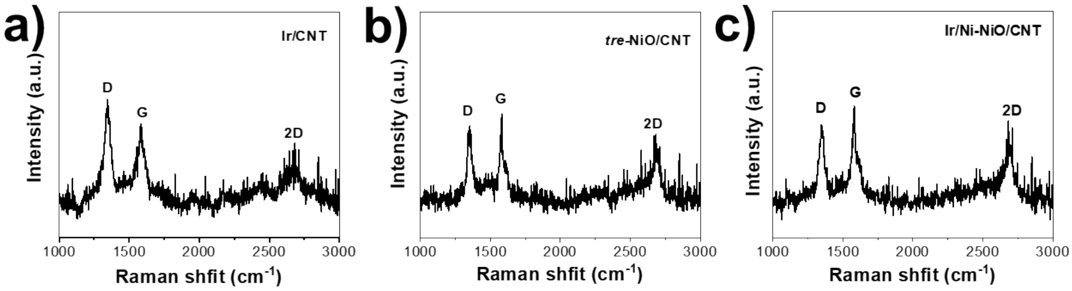

Fig. S6. Raman spectra of a) Ir/CNT. b) *tre*-NiO /CNT. c) Ir/Ni-NiO/CNT. The higher G and 2D band intensity of catalysts suggests a higher graphitization degree.

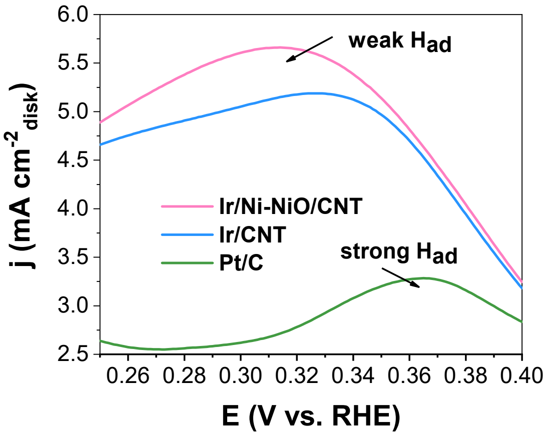

Fig. S7. Enlarged CV curves of Ir/Ni-NiO/CNT, Ir/CNT and Pt/C in Ar-saturated 0.1M KOH solution.

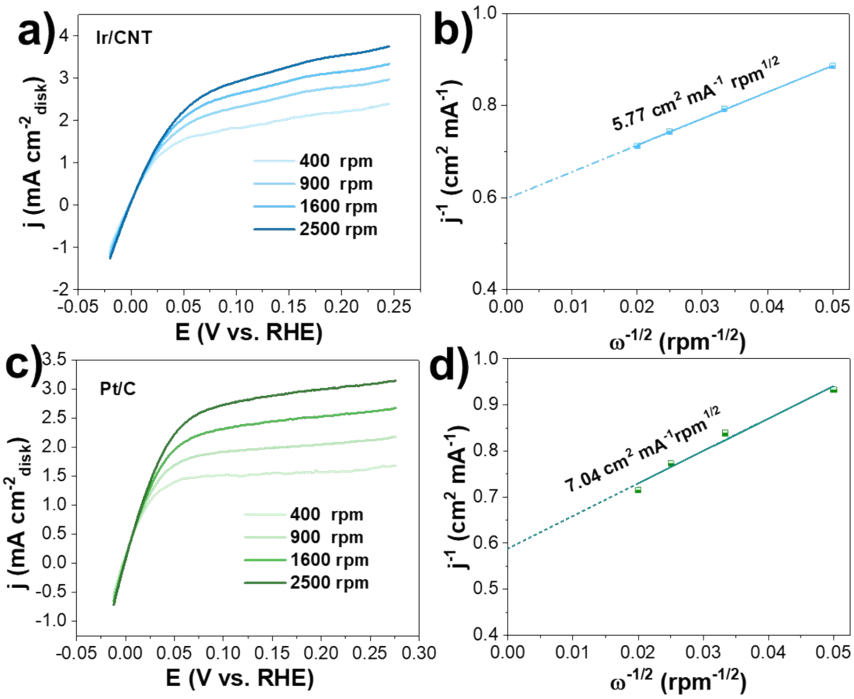

Fig. S8. HOR polarization curves in H_2-saturated 0.1 M KOH at various rotating rates and the corresponding Koutecky-Levich plots at 25 mV (vs RHE). a-b) Ir/CNT. c-d) Pt/C.

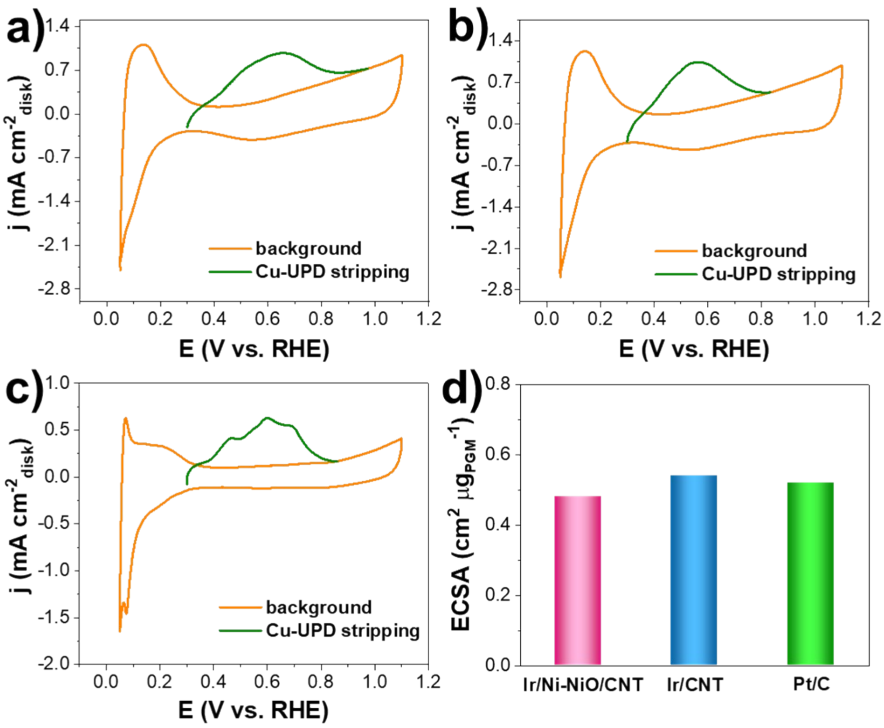

Fig. S9. Cu-UPD stripping voltammograms of Ir/Ni-NiO/CNT a), Ir/CNT b) and Pt/C c). The scan rates are 10 mV s^{-1}. d) ECSAs of these three catalysts.

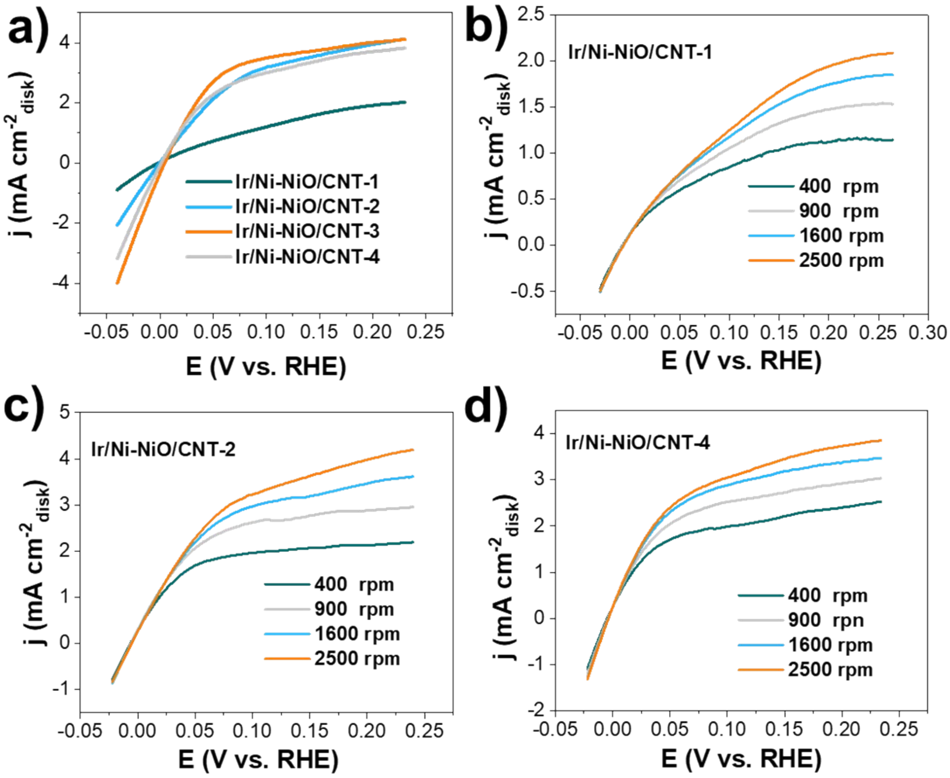

Fig. S10. a) HOR polarization curves of Ir/Ni-NiO/CNT at different loadings of Ir species and the corresponding HOR polarization curves in H_2-saturated 0.1 M KOH at various rotating rates. b) Ir/Ni-NiO/CNT - 1, c) Ir/Ni-NiO/CNT - 2 and d) Ir/Ni-NiO/CNT - 4.

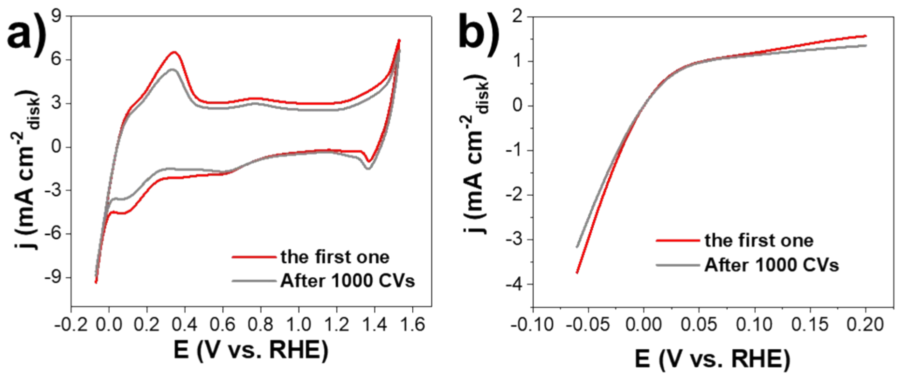

Fig. S11. a) CV curves in H_2-saturated 0.1 M KOH solution at a scan rate of 50 mV s^{-1}. b) HOR polarization curves in H_2-saturated 0.1 M KOH solution with a scan rate of 10 mV s^{-1} at a rotating rate of 2500 rpm of Ir/Ni-NiO/CNT before and after 1000 CV cycles.

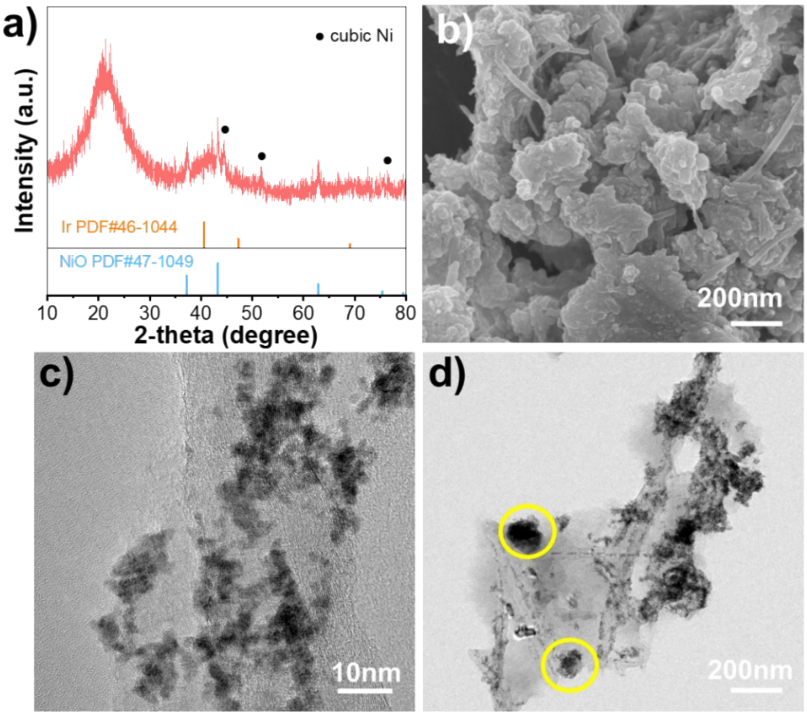

Fig. S12. Characterization results of the used catalyst for HOR. a) XRD pattern, b) SEM image, c-d) TEM images. The noted area shows the particle-like Ir/Ni-NiO unit.

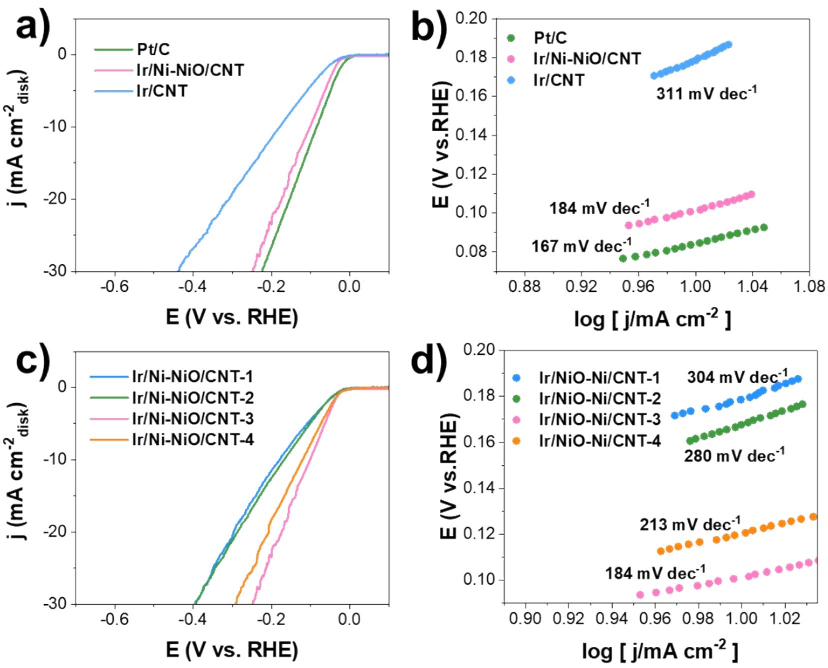

Fig. S13. a, c) HER polarization curves of Ir/Ni-NiO/CNT and other electrocatalysts. b, d) the corresponding HER Tafel slopes.

Supplementary tables

Table S1. ICP-AES data of different materials.

Catalysts	Ir(wt%)	Ni(wt%)
tre-NiO/CNT	/	43.6%
Ir/CNT	20.7%	/
Ir/Ni-NiO/CNT-1	2.0%	21.6%
Ir/Ni-NiO/CNT-2	3.6%	16.1%
Ir/Ni-NiO/CNT-3	9.17%	11.6%
Ir/Ni-NiO/CNT-4	11.2%	2.07%

Table S2. Summary of ECSA, j^k, j^0, $j^{k,m}$, $j^{0,m}$ and $j^{0,s}$ of various catalysts.

Catalysts	ECSA (cm^2 μg_{Ir}^{-1})	$j^k_{@50mV}$ (mA cm_{disk}^{-2})	$j^{k,m}_{@50mV}$ (mA $\mu g_{Ir\ or\ Pt}^{-1}$)	j^0 (mA cm_{disk}^{-2})	$j^{0,m}$ (A $g_{Ir\ or\ Pt}^{-1}$)	$j^{0,s}$ (μA $cm_{Ir\ or\ Pt}^{-2}$)
Ir/Ni-NiO/CNT	0.48	4.63	1.59	2.04	69.78	145
Ir/ CNT	0.54	2.99	0.45	1.58	24.01	44
Pt/C	0.52	3.23	0.51	1.59	25.00	48

Table S3. Benchmark HOR activities and the relevant parameters of catalysts in alkaline electrolytes.

Catalysts	Loading (μg_{PGM} cm_{disk}^{-2})	ECSA (cm^2 μg_{PGM}^{-1})	j^0 (mA cm_{disk}^{-2})	$j^{k,m}$ (mA μg_{Ir}^{-1}) at 50 mV	Refs.
Ir/Ni-NiO/CNT	29.46	0.48	2.04	1.59	This work
Ir/CNT	65.89	0.54	1.58	0.45	This work
Ir/C	2.44	0.49	0.67	0.67	S5
IrRu Nanowires/C	33.6	0.528	0.126	1.41	S6
Ir_9Ru_1/C	3.5	/	0.9	0.37	S7
Ir_3PdRu_6/C	3.5	/	0.6	0.34	S7
IrNi@Ir/C	10	0.48	1.22	1.12	S8
IrNi/C	10	0.41	0.90	0.77	S8
Ir/C	10	0.138	0.53	/	S2
Pt/C	63.69	0.52	1.59	0.51	This work

Supplementary references

S1. W. C. Sheng, H. A. Gasteiger and S. H. Yang, J. Electrochem. Soc., 2010, 157, B1529-B1536.

S2. J. Zheng, Z. B. Zhuang, B. J. Xu and Y. S. Yan, ACS Catal., 2015, 5, 4449-4455.

S3. J. Durst, A. Siebel, C. Simon, F. Haschéet, J. Herranzal and H. A. Gasteiger, Energy Environ Sci., 2014, 7, 2255-2260.

S4. L. H. Fu, F. L. Yang, Y. C. Hu, Y. B. Li, S. G. Chen and W. Luo, Sci. Bull., 2020, 65, 1735-1742.

S5. Y. Yang, X. D. Sun, G. Q. Han, X. Liu, X. Y. Zhang, Y. F. Sun, M. Zhang, Z. Cao and Y. Sun, Angew. Chem. Int. Ed., 2019, 58, 10644-10649.

S6. B. W. Qin, H. M. Yu, X. Q. Gao, D. W. Yao, X. Y. Sun, W. Song, B. L. Yi and Z. G. Shao, J. Mater. Chem. A., 2018, 6, 20374-20382.

S7. H. S.Wang and H. D. Abruna, J. Am. Chem. Soc., 2017, 139, 6807-6810.

S8. D. Liu, S. Q. Lu, Y. R. Xue, Z. Guan, J. J. Fang, W. Zhu and Z. B Zhuang, Nano Energy, 2019, 59, 26-32.